Published OnlineFirst July 27, 2020; DOI: 10.1158/1078-0432.CCR-19-2597

Tumor Subtype Determines Therapeutic Response to Chimeric Polypeptide Nanoparticle–based Chemotherapy in *Pten*-deleted Mouse Models of Sarcoma

Rebecca D. Dodd[1], Amanda Scherer[1], Wesley Huang[2], Gavin R. McGivney[1], Wade R. Gutierrez[1,3], Emily A. Laverty[1], Kathleen A. Ashcraft[2], Victoria R. Stephens[1], Parisa Yousefpour[4], Soumen Saha[4], Vickie Knepper-Adrian[1], Warren Floyd[2,5], Mark Chen[2,5], Yan Ma[2], Eric M. Mastria[4,5], Diana M. Cardona[6], William C. Eward[7], Ashutosh Chilkoti[4], and David G. Kirsch[2,8]

ABSTRACT

Purpose: Nanoparticle-encapsulated drug formulations can improve responses to conventional chemotherapy by increasing drug retention within the tumor and by promoting a more effective antitumor immune response than free drug. New drug delivery modalities are needed in sarcomas because they are often chemoresistant cancers, but the rarity of sarcomas and the complexity of diverse subtypes makes it challenging to investigate novel drug formulations.

Experimental Design: New drug formulations can be tested in animal models of sarcomas where the therapeutic response of different formulations can be compared using mice with identical tumor-initiating mutations. Here, using Cre/loxP and CRISPR/Cas9 techniques, we generated two distinct mouse models of *Pten*-deleted soft-tissue sarcoma: malignant peripheral nerve sheath tumor (MPNST) and undifferentiated pleomorphic sarcoma (UPS). We used these models to test the efficacy of chimeric polypeptide doxorubicin (CP-Dox), a nanoscale micelle formulation, in comparison with free doxorubicin.

Results: The CP-Dox formulation was superior to free doxorubicin in MPNST models. However, in UPS tumors, CP-Dox did not improve survival in comparison with free doxorubicin. While CP-Dox treatment resulted in elevated intratumoral doxorubicin concentrations in MPNSTs, this increase was absent in UPS tumors. In addition, elevation of $CD8^+$ T cells was observed exclusively in CP-Dox–treated MPNSTs, although these cells were not required for full efficacy of the CP nanoparticle–based chemotherapy.

Conclusions: These results have important implications for treating sarcomas with nanoparticle-encapsulated chemotherapy by highlighting the tumor subtype–dependent nature of therapeutic response.

Introduction

Soft-tissue sarcomas (STS) are mesenchymal tumors arising from connective tissues, including the muscle, adipose, and nerve sheath. These tumors are highly aggressive, with 1-year overall survival of 50%–60% for patients with advanced or metastatic disease (1). Primary sarcomas are frequently treated with radiotherapy and surgical resection, and chemotherapy is utilized to treat metastatic disease. Doxorubicin is the most common chemotherapy for advanced stage sarcoma (2–4). However, response rates are low, and there are significant risks for cardiac toxicity associated with high cumulative doses of doxorubicin. There are over 50 different subtypes of STS characterized by distinct genetic profiles, cells of origin, tissue histology, and tumor biology. Because of the rarity of each subtype, it is challenging to develop tailored treatment options for specific subtypes. Comparing the therapeutic response of distinct tumor subtypes with standard and novel therapies could help tailor treatment options for patients with different types of sarcoma. Two of the most aggressive forms of STS are undifferentiated pleomorphic sarcoma (UPS) and malignant peripheral nerve sheath tumor (MPNST). UPS is one of the most commonly diagnosed STS in adult patients and invades into the surrounding muscle. MPNSTs arise from the myelinating nerve sheath and occur in both adult and pediatric patients. Both sarcoma subtypes have complex karyotypes and harbor similar genetic alterations, including inactivation of a canonical tumor suppressor (*TRP53* or *CDKN2A)* and activation of the Ras pathway, usually through loss of the Ras GAP neurofibromin (*NF1*; refs. 5, 6).

Despite modest efficacy, doxorubicin is still considered a gold standard in sarcoma chemotherapy, although the response rate for single-agent doxorubicin remains low at 17%–27% (7). First-line therapy regimens for patients with both UPS and MPNST include adriamycin, an injectable form of doxorubicin hydrochloride. Because of the low chemoresponsiveness and significant cumulative cardiac toxicities, drug delivery formulations are being developed to increase bioavailability to the tumor and lower effective dose to some normal tissues. One nanoparticle-encapsulated approach is based on chimeric polypeptide (CP) technology. The CP consists of two segments: an elastin-like polypeptide (ELP) domain and a drug attachment domain at the C-terminus (8–10). Multiple copies of small-molecule drugs are conjugated to the drug attachment domain of the CP through an acid-labile linker. When the hydrophobicity of the drug is above a critical

[1]Department of Internal Medicine, University of Iowa, Iowa City, Iowa. [2]Department of Radiation Oncology, Duke University School of Medicine, Durham, North Carolina. [3]Medical Scientist Training Program, University of Iowa, Iowa City, Iowa. [4]Department of Biomedical Engineering, Duke University, Durham, North Carolina. [5]Medical Scientist Training Program, Duke University School of Medicine, Durham, North Carolina. [6]Department of Pathology, Duke University School of Medicine, Durham, North Carolina. [7]Department of Orthopedic Surgery, Duke University School of Medicine, Durham, North Carolina. [8]Department of Pharmacology & Cancer Biology, Duke University School of Medicine, Durham, North Carolina.

Note: Supplementary data for this article are available at Clinical Cancer Research Online (http://clincancerres.aacrjournals.org/).

Corresponding Authors: Rebecca D. Dodd, University of Iowa, 285 Newton Rd, 3269C CBRB, Iowa City, IA 52242. Phone: 319-335-4962, E-mail: rebecca-dodd@uiowa.edu; and David G. Kirsch, david.kirsch@duke.edu

Clin Cancer Res 2020;26:5036–47

doi: 10.1158/1078-0432.CCR-19-2597

Published OnlineFirst July 27, 2020; DOI: 10.1158/1078-0432.CCR-19-2597

Translational Relevance

Soft-tissue sarcomas (STS) are aggressive tumors of the connective tissue. Despite low response rates and cardiac toxicity, doxorubicin is still considered a gold standard in sarcoma chemotherapy. Nanoparticle-encapsulated drug formulations may provide improved responses and decreased toxicity to conventional chemotherapy in STS. Here, we examine the efficacy of an experimental nanoparticle-encapsulated doxorubicin formulation (CP-Dox) in two distinct types of STS using primary mouse models. The CP-Dox formulation improves survival in mice with malignant peripheral nerve sheath tumors (MPNST) compared with free doxorubicin, but has no survival benefit in mice with undifferentiated pleomorphic sarcoma (UPS). Pharmacokinetic studies indicate improved biodistribution in CP-Dox–treated MPNSTs, but not in UPS tumors. In addition, $CD8^+$ T cells are elevated in CP-Dox–treated MPNSTs, although these cells are not required for full efficacy of the CP nanoparticle–based chemotherapy. These results highlight the tumor subtype–specific events that define therapeutic response to nanoparticle-encapsulated chemotherapies.

threshold, drug conjugation triggers self-assembly of the CP into approximately 50-nm-diameter nanoparticles, with the drug sequestered in the core of the nanoparticle. Uptake of these nanoparticles by tumor cells and subsequent trafficking through the endolysosomal pathway results in cleavage of the drug from the ELP, followed by diffusion into the cytosol and transportation to its ultimate intracellular site of action. *In vivo*, systemically injected CP–drug conjugate nanoparticles accumulate in the tumor at a higher concentration than free drug due to the altered permeability of cancer-associated vasculature that allows nanoparticles to accumulate within tumor tissues, a phenomenon known as enhanced permeability and retention (EPR; ref. 11). Studies in a wide range of transplanted mouse models have shown these CP–nanoparticle formulations are superior to free drug with multiple agents, including doxorubicin (8–10, 12), paclitaxel (13), and niclosamide (14). In addition to improved survival, increased tumor uptake, and decreased cardiac toxicity, these agents can also increase T-cell infiltration into treated tumors, an event that is critical to drug efficacy in syngeneic mouse models (15).

Genetically engineered mouse models have advanced our molecular understanding of sarcomas and serve as useful preclinical platforms for multiple subtypes of STS. We have previously examined chemotherapy regimens in mouse models of MPNST and UPS, and we demonstrated that these models have low response rates to traditional doxorubicin formulations (16–18). These sarcoma mouse models use Cre/loxP technology to spatially and temporally restrict tumorigenesis. This approach uses exogenous delivery of an adenovirus expressing Cre recombinase (Ad-Cre) to delete floxed genes at the site of Ad-Cre injection. By altering the site of Ad-Cre delivery, we have used this technology to generate high-fidelity models of distinct subtypes of sarcoma, including MPNST (via sciatic nerve injection of Ad-Cre) and UPS (via muscle injection of Ad-Cre; refs. 19, 20). We demonstrated that Ad-Cre injection into the sciatic nerve of $Nf1^{Flox/Flox}$; $Cdkn2a^{Flox/Flox}$ mice (NC mice) generates MPNSTs at the site of injection within 3–4 months, while injection into the gastrocnemius muscle of NC mice generates UPS tumors within 7–9 months (17). These models facilitate preclinical studies because tumor location is easily monitored and measured by calipers. Importantly, these primary mouse models arise within a native tumor microenvironment, facilitating studies on tumor vasculature and immune infiltration. Because NC mice can generate either MPNST or UPS, these models provide a unique opportunity to directly compare the preclinical efficacy of novel therapeutic approaches in different sarcoma tumor contexts using genetically identical mice.

While the latency for MPNSTs to develop in NC mice is relatively short, the 7–9 month time frame for UPS tumor development in NC mice is a limitation for preclinical studies. To shorten the initiation time required for *Nf1/Cdkn2a*-null UPS tumors for preclinical studies, we explored additional patient-relevant mutations that could accelerate UPS formation in this model. Dysregulation of the PI3K/AKT/mTOR signaling axis is common across multiple sarcoma types (5, 21) and correlates with poor response to treatment (22). Both IHC and gene expression studies have shown that PTEN expression can be lost in patient samples of aggressive MPNST and UPS through DNA methylation or copy-number loss (5, 23, 24). Data from multiple groups demonstrate that combining *Pten* deletion with loss of either *p53* or *Nf1* can generate several distinct types of STS in genetically engineered mice, including leiomyosarcoma (25), UPS (26), or MPNST (24, 27). For example, high-grade peripheral nerve sheath tumors were generated in $Pten^{Flox/Flox}$; $Nf1^{Flox/Flox}$ mice with Schwann cell–specific expression of Cre recombinase (27). However, these mice died within 20 days of birth due to aggressive tumor burden. On the basis of these data, we hypothesized that introducing somatic *Pten* loss into the NC mouse models would accelerate tumor development to enhance the feasibility of longitudinal preclinical studies. Here, we describe Cre/loxP and CRISPR/Cas9 approaches to generate new spatially and temporally restricted models of *Pten*-deleted sarcoma that can serve as accelerated preclinical platforms.

To determine whether CP nanoparticle–based chemotherapy is a promising therapeutic approach for STS, we tested the efficacy of CP-nanoparticle doxorubicin (CP-Dox) in MPNST and UPS mouse models containing identical tumor-initiating mutations. While MPNST-bearing mice show improved survival after treatment with CP-Dox in comparison with free doxorubicin, UPS-bearing mice have similar responses to both free doxorubicin and CP-Dox formulations. The juxtaposition of two models that demonstrate different survival benefits from CP-Dox allows for investigations into possible mechanisms driving this response. We observed improved biodistribution in MPNSTs treated with CP-Dox, but not in CP-Dox–treated UPS tumors. In addition, we observed elevated $CD8^+$ T-cell infiltration exclusively in CP-Dox–treated MPNSTs, although these cells were not required for full efficacy of the CP nanoparticle–based chemotherapy.

Materials and Methods

Animals

$Nf1^{Flox/Flox}$; $Cdkn2a^{Flox/Flox}$ mice were described previously (17). $Pten^{Flox/Flox}$ mice (28) and the *Rosa26-LSL-Cas9* mice (29) were obtained from Jackson laboratories. All animal experiments were performed in accordance with protocols approved by IACUC at Duke University (Durham, NC), and the University of Iowa (Iowa City, IA).

Tumor generation and growth analysis

Cre/loxP tumors were generated as previously described for UPS and MPNST models (30). Briefly, Ad-Cre (University of Iowa Viral Vector Core, Iowa City, Iowa) was mixed with calcium phosphate as described previously (19). The mixture of calcium phosphate/Ad-Cre was incubated for 15 minutes at room temperature and injected into

Published OnlineFirst July 27, 2020; DOI: 10.1158/1078-0432.CCR-19-2597

the lower leg (50 μL) or sciatic nerve (25 μL) to generate UPS or MPNSTs, respectively. CRISPR/Cas9 tumors were generated as described previously (31). Virus containing Cre and single-guide RNAs (sgRNA) for Pten or Tomato control were generated by ViraQuest. sgRNA sequences were described previously (32). After tumors were detected, mice were measured three times weekly by calipers to obtain tumor growth kinetics data as described previously (17). Tumor volumes were calculated using the formula $V = (\pi \times L \times W \times H)/6$, with L, W, and H representing the length, width, and height of the tumor in mm, respectively. Tumors were harvested when they reached 1,500 mm^3 or when animals showed signs of distress. At sacrifice, primary tumor tissue was collected for cell line generation or placed into 10% formalin for histology.

Indel analysis

PCR amplification of a region of mouse *Pten* spanning the sgRNA target site was performed using Phusion High-Fidelity DNA Polymerase (NEB, M0530L). PCR amplicons were validated on a 2% agarose gel and then purified with the Monarch PCR and DNA Cleanup Kit (NEB, T1030S). Sanger sequencing was performed by the Genomics Division of the Iowa Institute of Human Genetics at the University of Iowa (Iowa City, IA). Chromatograms were analyzed using Synthego ICE (ice.synthego.com) or TIDE (tide.deskgen.com). Indel frequencies were quantified using sequence trace analysis. Indels >50 base pairs (bp) were determined by band size on a 2% agarose gel. PCR primers for *Pten* indels generated a 778 bp fragment in wild-type tissue that flanks the Pten sgRNA target site (Fw 5′CTGTCACCATTGCCAGGGCT, Rv 5′ATTTTAAGAAGAGACCACAGAGCTCGAC).

In vivo doxorubicin studies

Tumors within a uniform size range (150–300 mm^3) were treated with PBS control or doxorubicin formulations. Each doxorubicin formulation was given at the MTD. For free doxorubicin, mice were treated intraperitoneal with a single bolus of 10 mg/kg. CP-Dox was synthesized as described previously (8–10, 12, 15), and mice were injected with a single bolus in the tail vein (20 mg/kg). Briefly, CPs were synthesized by expression of a plasmid-borne synthetic gene of the CP in *E. coli*. Activated doxorubicin was covalently linked to cysteine residues on the CP with n-ßmaleimidopropionic acid hydrazide. To further purify the nanoparticles, the ELP phase transition was initiated with sodium chloride (2.5 mol/L) to trigger phase transition of the CP-Dox conjugate into an aqueous immiscible phase, followed by centrifugation at 4,000 rpm at 30°C for 20 minutes. The concentration of doxorubicin was determined using the absorbance at 495 nm and the doxorubicin molar extinction coefficient of 1.00×10^4 mol/L^{-1} cm^{-1}. Tumor growth was determined by caliper measurement three times weekly. Following sacrifice, tumor tissue was collected for histochemical analysis.

Pharmacokinetics and biodistribution studies

Measurement of pharmacokinetics and biodistribution were performed as described previously (8–10, 12, 15). Briefly, 5 mg/kg of free doxorubicin or CP-Dox was injected intravenously via the tail vein, and samples were obtained from the tumor, kidney, and muscle at 2 and 24 hours after injection. Tumors were weighed, and doxorubicin was extracted by homogenizing samples in acidified isopropanol with 2-mm zirconia beads and a MiniBeadbeater-1TM (Biospec). Samples were incubated overnight in acidified isopropanol at 4°C, vortexed, and centrifuged (14,000 rpm, 10 minutes, 4°C). The amount of fluorescent doxorubicin in the supernatant was quantified using 485 nm for excitation and 590 nm for emission. For each sample, the background fluorescence was subtracted according to calibration curves made for each organ, and the remaining counts were converted to drug concentration using a doxorubicin fluorescence standard curve, as described previously (33). Tumor values were normalized to kidney and muscle, as these provided the most consistent baseline references.

$CD8^+$ T-cell depletion studies

NC mice with tumors within a uniform size range (150–300 mm^3) were injected with 200 μg of anti-CD8α (53–6.72, Bio X Cell) or rat IgG2a isotype control (2A3, Bio X Cell) starting on the day that each tumor was first identified (150–300 mm^3), and continuing twice per week until the study endpoint. Twenty-four hours after antibody delivery, mice were administered either CP-Dox or PBS control, as described above. Tumor growth was determined by caliper measurement three times weekly. For flow cytometry analysis, tumor tissue was stained with antibodies against CD45 (BV605, 30F11), CD11b (PE, M1/70), CD11c (BV421, N418), CD3e (PE-Cy7, 145-2C11), CD4 (AF700, GK1.5), and CD8 (PerCP Cy5.5, 53-6.7) and analyzed by flow cytometry. All flow cytometry reagents were purchased from Biolegend.

IHC

Upon sacrifice, a portion of tumor tissue was harvested within 30 minutes and stored in 10% neutral buffered formalin for fixation and subsequent paraffin embedment. Antibodies for IHC were used at 1:200 and include pERK (Cell Signaling Technology, clone D13.14.4E), pS6 (Cell Signaling Technology, clone D68F8), CD4 (Abcam, clone 183685), and CD8 (Thermo Fischer Scientific, clone 4SM15). Sections were deparaffinized in xylene and rehydrated through a series of ethanol washes. Antigen retrieval was performed in citrate-based buffer (Vector Labs). After washing, samples were stained using VECTASTAIN Elite ABC-HRP kit, as per the manufacturer's instructions (Vector Labs). Slides were counterstained using IHC-optimized hematoxylin (Vector Labs). Sections were dehydrated and mounted with Permount. Quantification of immune cell staining was performed on six 20× fields selected from at least three individual sections to generate the total number of positively stained cells.

Western blot analysis

Tumor cell lines were lysed in ice-cold RIPA buffer supplemented with protease and phosphatase inhibitors (Thermo Fisher Scientific, 89900, A32961). Protein concentration was determined by BCA assay (Thermo Fisher Scientific, 23225) and samples were loaded into 12%–4% Bis-Tris Plus gels (Thermo Fisher Scientific, NW04120Box) and then transferred to polyvinylidene difluoride Immobilon-FL membranes (Millipore, IPFL00010). Membranes were incubated overnight at 4°C with primary antibodies: pAkt, 1:1,000 (4060, Cell Signaling Technology); pErk, 1:1,000 (4370, Cell Signaling Technology), pS6, 1:1,000 (5364, Cell Signaling Technology), γ-Tubulin, 1:10,000 (T5326, Sigma-Aldrich), Erk, 1:1000 (9102, Cell Signaling Technology), Akt, 1:1000 (4685, Cell Signaling Technology), and RPS6, 1:1000 (Ab40820, Abcam). Membranes were incubated with secondary antibodies for 1 hour at room temperature: goat anti-rabbit IRDye800 (1:5,000 LI-COR, 926-3221) and donkey anti-mouse IRDye680 (1:10,000 LI-COR, 926-68072). Membranes were imaged using an Odyssey CLx (LI-COR) and image analysis was performed using Image Studio Software (LI-COR).

Published OnlineFirst July 27, 2020; DOI: 10.1158/1078-0432.CCR-19-2597

IC_{50} Analysis

Cells were seeded onto a 96-well plate at a concentration of 1,000 cells/well and treated with either CP-Dox or free doxorubicin using three replicate wells per drug concentration. Treatment concentrations started at 500 μmol/L and were serially diluted at a 1:2 ratio. Immediately following administration of therapeutic agent, cells were placed in the Incucyte Zoom live cell imaging system, where four locations on each well of the 96-well plate were serially imaged every 2 hours for 3 days. After the experiment was completed, a phase filter was created to allow quantification of percent confluence for each well at each time point. IC_{50} values for each plate was determined using AUC analysis in the PRISM 7 software (Graphpad).

Statistical analysis

Statistical analysis was performed using the Prism 7 software (GraphPad), and a $P < 0.05$ was considered statistically significant. Kaplan–Meier survival curves were analyzed by Gehan–Breslow–Wilcoxon test. Analysis of tumor growth kinetics and immune infiltration studies was performed by one-way ANOVA with Tukey multiple comparison test, with Bonferroni adjustment. Biodistribution data were analyzed by ordinary two-way ANOVA.

Results

Cre/loxP and CRISPR/Cas9 mouse models of Pten-deleted sarcomas

To generate primary mouse models of STS to undertake preclinical therapeutic studies of CP nanoparticle–based chemotherapy in MPNSTs and UPS tumors, we chose to accelerate tumorigenesis in the previously described NC model (17) by introducing *Pten* loss-of-function mutations. We used two parallel genetic approaches to generate *Pten*-deleted sarcoma models in genetically engineered mice (Supplementary Fig. S1). First, we used a traditional Cre/loxP approach by crossing $Pten^{Flox/Flox}$ mice with NC mice to generate $Pten^{Flox/Flox}$; $Nf1^{Flox/Flox}$; $Cdkn2a^{Flox/Flox}$ animals ($Pten^{Flox/Flox}$; NC mice). Following injection with Ad-Cre into either the sciatic nerve or muscle, the $Pten^{Flox/Flox}$; NC mice developed MPNST or UPS, respectively (**Figs. 1A** and **2A**). Second, we applied our newly developed CRISPR/Cas9 somatic tumorigenesis technology to create complementary models of spatially and temporally restricted *Pten*-deleted sarcoma (**Figs. 1B** and **2B**). We recently used this approach to deliver adenovirus containing Cas9 and sgRNAs to generate STS models that closely resemble tumors generated by Cre/loxP methods (31). In this study, we adapted this approach to deliver *Pten*-directed sgRNAs into NC mice containing a Cre-inducible Cas9 (*Rosa26-LSL-Cas9*), which allows for localized activation of Cas9 at the site of injection (29). By using a combination of approaches, we can compare models generated by traditional Cre/loxP methods with more versatile CRISPR/Cas9 approaches.

Somatic Pten deletion accelerates MPNST tumorigenesis

To use Cre/loxP to induce MPNSTs with deletion of *Pten*, we injected the sciatic nerve of $Pten^{Flox/Flox}$; NC mice with Ad-Cre to delete *Pten, Nf1*, and *Cdkn2a* in the nerve sheath. In comparison with mice with wild-type *Pten* (NC mice) or heterozygous deletion of *Pten* ($Pten^{Flox/+}$; NC mice), homozygous deletion of *Pten* accelerated MPNST initiation to an average of 69 days after injection (**Fig. 1A**). In contrast, NC mice with intact *Pten* required an average of 114 days for tumor formation, which is similar to our previously reported tumor latency for this model (17). To utilize CRISPR/Cas9 technology to mutate Pten in the NC MPNST model, we generated mice with a Cre-activatable Cas9 (*Rosa26-LSL-Cas9*) and floxed *Nf1* and *Cdkn2a* alleles (*Rosa26-LSL-Cas9; Nf1*$^{Flox/Flox}$; *Cdkn2a*$^{Flox/Flox}$, referred to as LSL-Cas9; NC mice). Ad-Cre injection into these mice activates Cas9 expression by deletion of the upstream floxed STOP cassette, as well as deleting the floxed genes *Nf1* and *Cdkn2a*. This adenovirus also contains sgRNAs for either *Pten* (Ad-Cre + sgPten) or a negative control designed against a nonexpressed fluorescent Tomato protein (Ad-Cre + sgTom). When LSL-Cas9; NC mice are injected in the sciatic nerve with Ad-Cre + gPten, *Nf1/Cdkn2a*-null tumors develop that express Cas9 targeting *Pten* disruption (**Fig. 1B**). As a negative control, LSL-Cas9; NC mice are injected with Ad-Cre + sgTom, which does not target Cas9 to a specific sequence in the mouse genome. LSL-Cas9; NC mice injected with Ad-Cre + sgPten develop tumors more quickly than control mice injected with Ad-Cre + sgTom (52 vs. 93 days), similar to results seen with the Cre/loxP approach in **Fig. 1A**. To confirm *Pten* disruption in CRISPR/Cas9-initiated tumors, we performed indel pattern analysis on tumor-derived cell lines (**Fig. 1C**). This method examines the frequency and location of insertions and deletions within individual tumors generated by CRISPR/Cas9 targeting (34). For the three MPNST-derived cell lines in this study, we determined that deletions were more common than insertion events, and indels most frequently occurred within 1–10 bp of the cut site. We compared the impact of *Pten* loss on tumor growth in both model systems by measuring tumor volume by caliper measurement. While deletion of *Pten* in the Cre/loxP model does not alter tumor growth kinetics, *Pten* mutation in the CRISPR/Cas9 model appears to accelerate the time required for MPNSTs to triple in volume (**Fig. 1D**). Histopathologic examination of tumors from both Cre/loxP and CRISPR/Cas9 approaches confirmed MPNST features (**Fig. 1E**). Taken together, these data are consistent with other studies of *Pten* deletion in nerve sheath tumors (24, 27), and provide robust new spatially and temporally restricted mouse models for preclinical studies of MPNST.

UPS initiation is accelerated by Pten loss

One limitation of our previously described *Nf1*-driven UPS model is the long tumor latency, making rigorous and moderate-throughput preclinical studies challenging. We and others have shown that the PI3K pathway plays an important role in UPS (16, 24–27), and we hypothesized that *Pten* deletion would accelerate tumor formation in the NC model. Using Cre/loxP technology, injection of Ad-Cre into the gastrocnemius muscle of NC or $Pten^{Flox/+}$; NC mice generates tumors with an average latency of 138 and 129 days, respectively. In contrast, deletion of two copies of *Pten* accelerates UPS latency to an average of 89.5 days (**Fig. 2A**). A similar phenotype is observed using the CRISPR/Cas9 model in LSL-Cas9; NC mice, where injection of Ad-Cre + gPten generates tumors in an average of 78 days, but only 2 of 12 LSL-Cas9; NC mice injected with the negative control sgRNA (Ad-Cre + sgTom) developed tumors after 5–8 months (**Fig. 2B**). This is longer than the time required for tumorigenesis in Cre/loxP-driven NC mice with wild-type *Pten*, suggesting that *Pten* deletion may play a larger role in tumorigenesis for mice with constitutive Cas9 expression. Indel pattern analysis shows that cell lines from CRISPR/Cas9-generated UPS tumors have a wide range of indels within *Pten*, including one tumor-derived cell line with a large deletion greater than 50 bp (**Fig. 2C**). Tumors generated by both methods show the classic spindle cell morphology commonly observed in UPS (**Fig. 2E**). Similar to observations in the MPNST model, deletion of *Pten* in Cre/loxP-generated UPS tumors does not alter tumor proliferation, while mutation of *Pten* via CRISPR/Cas9 technology appears to accelerate UPS growth kinetics in comparison with $Pten^{Flox/+}$; NC and NC

Published OnlineFirst July 27, 2020; DOI: 10.1158/1078-0432.CCR-19-2597

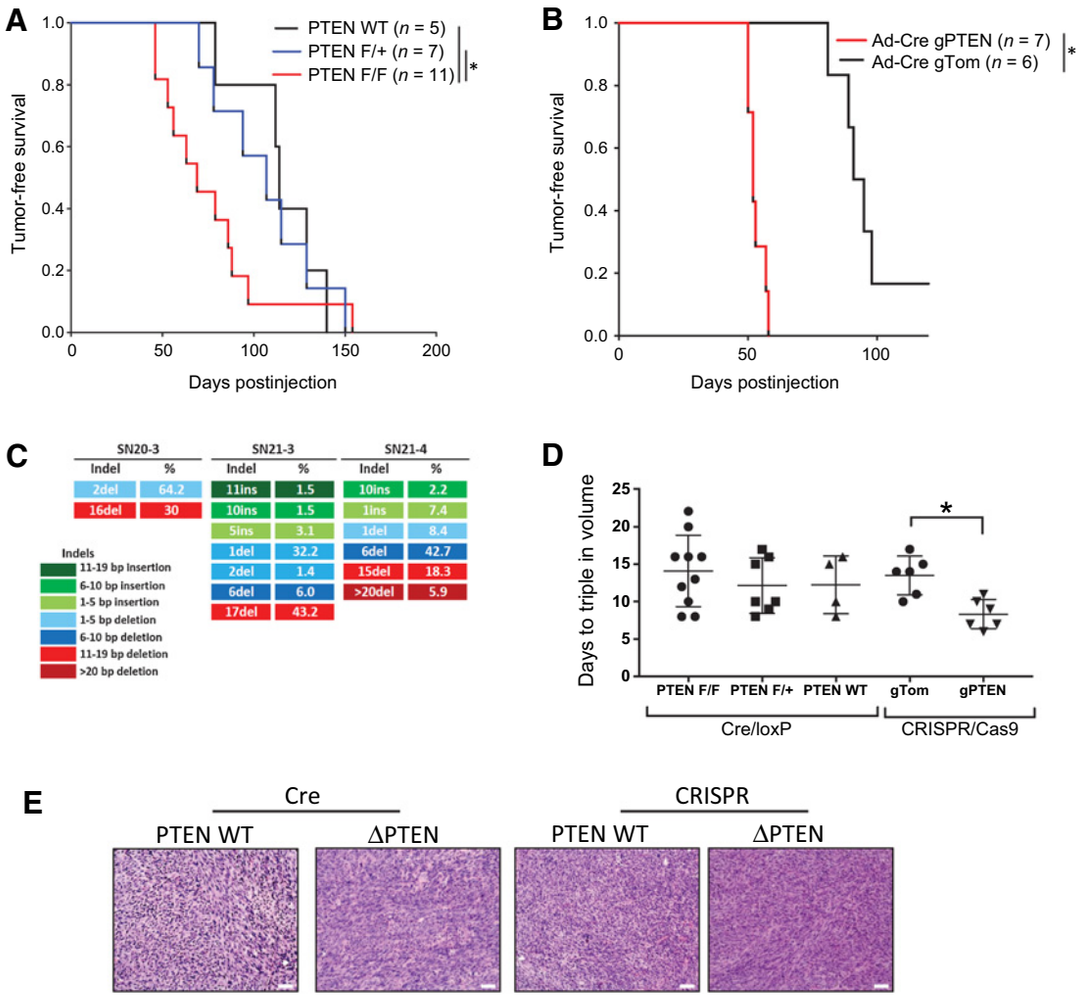

Figure 1.

Pten deletion accelerates MPNST formation. **A,** Cre/loxP homozygous deletion of *Pten* accelerates MPNST formation in $Nf1^{Flox/Flox}$; $Cdkn2a^{Flox/Flox}$ (NC) mice. No acceleration of tumor formation is seen in mice with loss of only a single *Pten* allele. **B,** Similarly, CRISPR-mediated mutation of *Pten* using a sgRNA targeting *Pten* in Rosa26-LSL-Cas9; NC mice leads to accelerated tumor formation when compared with a nontargeting guide RNA (gTom) against a fluorescent tdTomato gene. **C,** Indel pattern analysis shows the frequency and distribution of insertions and deletions in cell lines derived from tumors generated by injections of Ad-Cre + gPten. **D,** Tumor growth kinetics are reported as the number of days required for tumors to triple in volume. For the Cre/loxP model, PTEN deletion does not alter the tumor growth kinetics. However, loss of *Pten* in the CRISPR/Cas9 model accelerates tumor growth in comparison with a nontargeting sgRNA control ($P = 0.003$). **E,** Representative images of hematoxylin and eosin–stained tumors demonstrate MPNST pathology, which shows that deletion of *Pten* does not alter the histology of the tumors. Images at 20×, scale bar at 50 μm. A "*" denotes $P < 0.05$.

models (**Fig. 2D**). While it is interesting that deletion of *Pten* via CRISPR/Cas9 technology appears to accelerate tumor growth in both UPS and MPNST models, this phenotype requires further validation in a larger cohort of mice. Taken together, these data show that *Pten* deletion can accelerate tumor initiation in mouse models of two distinct sarcoma subtypes, and that CRISPR/Cas9 approaches to mutate *Pten* can accelerate sarcoma development similar to Cre/loxP-mediated deletion.

Pten-dependent cellular signaling in MPNST and UPS

Disruption of *Pten* results in pAKT elevation, which can drive cell proliferation and survival (35). In addition, PI3K signaling can modulate cross-talk with the MAPK/ERK and mTOR/S6 pathways (35, 36). These distinct signaling arms can play roles in sarcoma progression; however, their activation is context-dependent and may rely upon the presence of additional mutations or sarcoma subtype. To assess PI3K pathway activation in the *Pten/Nf1/Cdkn2a*-null sarcoma models, we used Western blots of tumor-derived cell lines to examine three frequently activated signaling nodes in the PI3K pathway: phospho-AKT, phospho-S6, and phospho-ERK. In MPNSTs, *Pten* deletion elevates phospho-AKT levels in cells derived from both Cre/loxP and CRISPR/Cas9 models (**Fig. 3A**). Western blot analysis of *Pten*-deleted MPNST cells shows elevation of phospho-S6 in cell lines derived from CRISPR/Cas9-generated tumors, whereas the induction of phospho-S6 is less pronounced in cell lines derived from Cre/loxP-initiated tumors. Moderate levels of phospho-ERK are observed in cell lines from MPNSTs by Western blot analysis, but we are unable to detect further induction of phospho-ERK with *Pten* deletion.

Published OnlineFirst July 27, 2020; DOI: 10.1158/1078-0432.CCR-19-2597

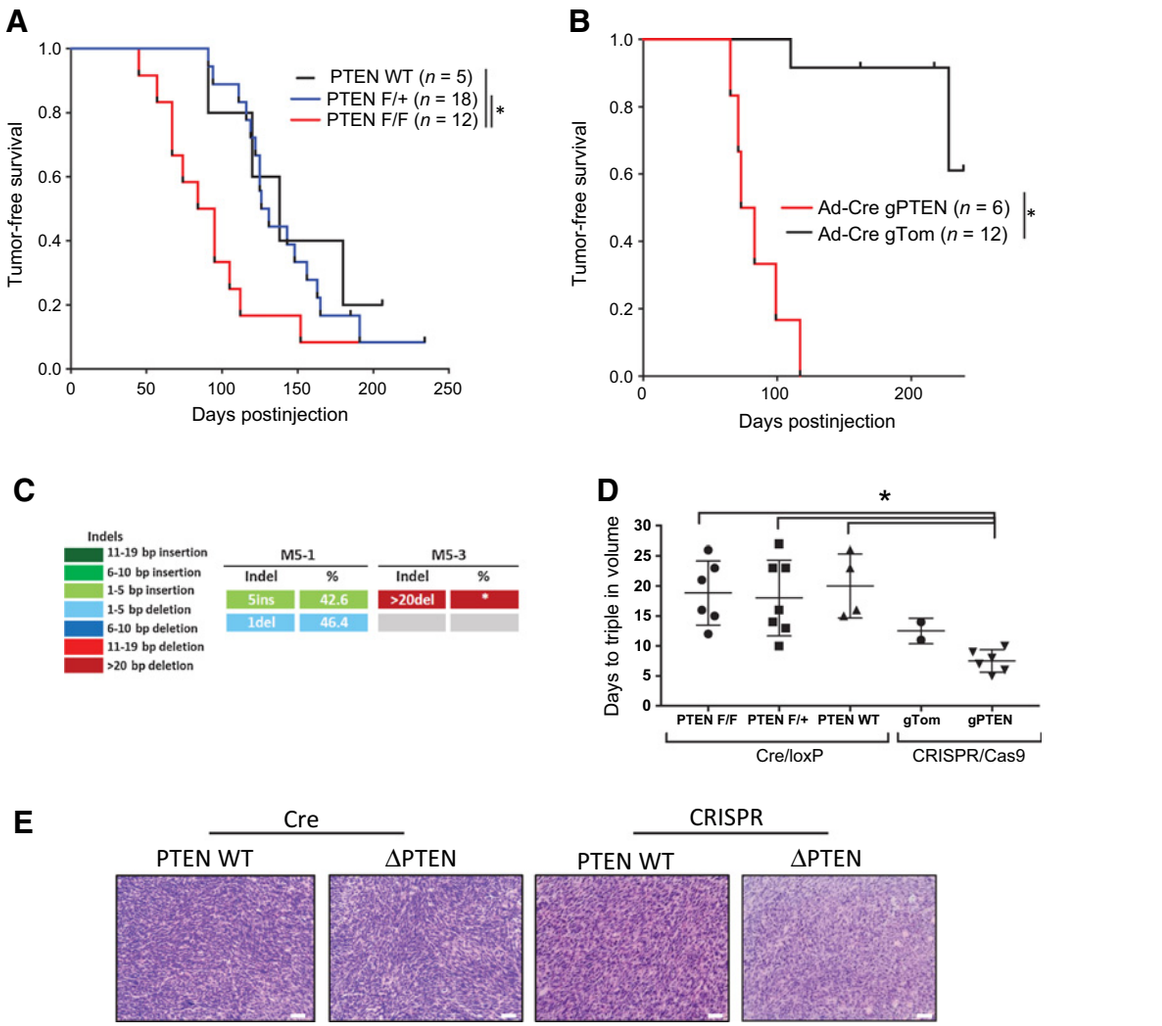

Figure 2.

Pten deletion accelerates UPS formation. **A,** UPS tumor formation is accelerated with Cre/loxP homozygous deletion of *Pten* in $Nf1^{Flox/Flox}$; $Cdkn2a^{Flox/Flox}$ (NC) mice. No acceleration of tumor formation is seen in mice with loss of only a single *Pten* allele. **B,** Mutation of *Pten* with a sgRNA in LSL-Cas9; NC mice leads to accelerated tumor formation when compared with a nontargeting sgRNA (gTom) against a fluorescent tdTomato gene. Because of the long duration required for tumors to grow, only two tumors were observed with the control sgRNA (gTom) injections. **C,** CRISPR/Cas9-generated indels in *Pten* were confirmed by Sanger sequencing of tumor-derived cell lines generated by injections of Ad-Cre + gPten. Indel pattern analysis shows the frequency and distribution of insertions and deletions. The deletion observed in M5-3 was too large to be sequenced with the primers using a Sanger sequencing–based approach, so the size of the deletion was estimated by agarose gel electrophoresis as at least 50 bp, denoted by an asterisk. **D,** Tumor growth kinetics are reported as the number of days required for tumors to triple in volume. Similar to observations in the MPNST model, deletion of *Pten* with Cre/loxP in UPS tumors does not affect tumor growth kinetics, but loss of *Pten* in the CRISPR/Cas9 model accelerates tumor growth in comparison with $Pten^{F/F}$, $Pten^{F/+}$, and Pten WT Cre/loxP models. **E,** Representative images of hematoxylin and eosin–stained tumors show classic UPS spindle cell morphology is preserved with *Pten* deletion in both Cre/loxP and CRISPR/Cas9 approaches. Images at 20×, scale bar at 50 μm. A "*" denotes $P < 0.05$.

Similar results are seen in UPS tumors. Western blot analyses show that deletion of *Pten* upregulates phospho-AKT levels in UPS-derived cell lines generated by both Cre/loxP and CRISPR/Cas9 approaches (**Fig. 3B**). In contrast, levels of phospho-S6 are modestly upregulated following *Pten* loss in cell lines from CRISPR/Cas9-derived UPS tumors, but show no consistent changes in cell lines from Cre/loxP-derived sarcomas. These results in UPS cell lines is similar to results seen in MPNST cell lines and suggests that the elevated mTOR/S6 activity in these tumors could contribute to accelerated growth kinetics in tumors with *Pten* deletion by CRISPR/Cas9 technology. In contrast to MPNST models, Western blots in cell lines from some UPS tumors with *Pten* loss demonstrate that levels of phospho-ERK are moderately upregulated. As these Western blots are examining tumor-derived cell lines, and not tumor lysates, it is possible the differences in pS6 and pERK levels between cell lines can be attriuted to additional mutations or epigenetic events that were gained during culture to select for divergent signaling properties. Alternatively, our results may reflect the heterogeneity of signaling profiles across individual tumors. Regardless, these results show that *Pten* loss activates the mTOR/S6 pathway through distinct tumor context-dependent events, suggesting unique cell signaling paradigms for different sarcoma subtypes.

Published OnlineFirst July 27, 2020; DOI: 10.1158/1078-0432.CCR-19-2597

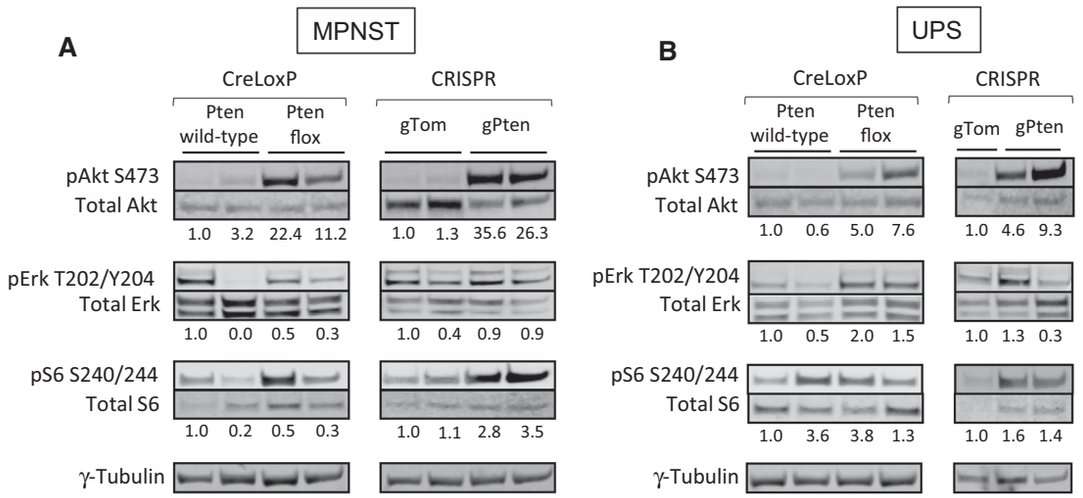

Figure 3.

The impact of *Pten* deletion on cellular signaling pathways is context-dependent. **A,** Western blots of key signaling pathways in MPNST-derived cell lines. Quantification is shown as fold change in phosphorylated protein compared with total protein, which is normalized to a *Pten* wild-type control. Elevation of phospho-AKT is observed in *Pten*-deleted samples obtained from both Cre/loxP and CRISPR/Cas9 approaches. Phospho-S6 levels are increased in *Pten*-deleted samples from CRISPR/Cas9 tumors, but not in cells derived from Cre/loxP tumors. Phospho-ERK levels are not altered by *Pten* deletion in either model. **B,** Western blots of key signaling pathways in UPS-derived cell lines. Quantification is shown as fold change in phosphorylated protein compared with total protein, which is normalized to a *Pten* wild-type control. Elevation of phospho-AKT is observed in *Pten*-deleted samples obtained from both Cre/loxP and CRISPR/Cas9 approaches. In UPS-derived cell lines, *Pten* loss modestly upregulates phospho-S6 in CRISPR/Cas9 tumors, but has no consistent impact on phospho-S6 levels in cell lines derived from Cre/loxP tumors. Phospho-ERK levels are elevated in cell lines from *Pten*-deleted Cre/loxP tumors, but not in cell lines from *Pten*-deleted CRISPR/Cas9 tumors.

CP-Dox improves survival in a primary mouse model of MPNST

Doxorubicin (adriamycin) is the most common first-line chemotherapy for patients with both MPNST and UPS, despite poor overall response rates. CP nanoparticle–encapsulated doxorubicin (CP-Dox) has improved bioavailability and extends survival in mouse cell transplantation models, but has not been tested in primary mouse models (8–10, 12–15, 37). The shortened latencies of the *Pten*-deleted MPNST and UPS models described above facilitate preclinical testing of CP-Dox. Given the success of CP-formulated drugs in mouse models of epithelial cancers (8–10, 12–15, 37), we hypothesized that CP-Dox would improve survival better than free doxorubicin in the MPNST and UPS sarcoma mouse models. We generated both MPNSTs and UPS tumors in $Pten^{Flox/Flox}$; NC mice, as these Cre/loxP mice were developed before the CRISPR/Cas9 models were available. After tumors reached 200 mm^3, mice were treated with a single administration of free doxorubicin or CP-Dox at MTDs, as reported previously (15). It is important to note that the comparison between free-doxorubicin and CP-Dox were performed not at equimolar amounts but at equitoxic doses—typically the MTD of each drug—as it allows for comparisons of clinically relevant doses. Tumor growth was monitored by calipers three times weekly. In MPNST-bearing mice, animals treated with vehicle alone have a median survival of 11 days. This is similar to the 14 days median survival for mice receiving free doxorubicin, demonstrating the lack of survival benefit with free drug formulation in this model (**Fig. 4A**). In contrast, CP-Dox extends median survival to 24 days, significantly longer than free doxorubicin or vehicle treatment (**Fig. 4A**). The nanoparticle-encapsulated formulation also slows tumor growth by increasing the average time required for tumors to double in volume from 4 days with vehicle treatment to 13.1 days with CP-Dox (**Fig. 4B**; Supplementary Fig. S2). To our knowledge, this is the first report of the CP-based nanoparticle delivery improving survival in a primary mouse model.

In the UPS model, treatment with free doxorubicin extends median survival to 44 days compared with 25 days with vehicle alone (**Fig. 4C**). However, there was no additional survival benefit with CP-Dox versus free doxorubicin (43 days vs. 47 days, respectively). Similar results are observed in tumor growth data, with both drug formulations extending the time required for tumors to double in volume from 7.4 days with vehicle alone to 23.4 and 21 days with free doxorubicin and CP-Dox, respectively (**Fig. 4D**; Supplementary Fig. S2). This is in contrast to the MPNST model, where only CP-Dox treatment improves survival (**Fig. 4A**). Thus, these data suggest CP-Dox can improve survival compared with free doxorubicin in MPNSTs because of the poor baseline response of MPNSTs to free doxorubicin, whereas CP-Dox is unable to extend survival in UPS tumors beyond the benefit already achieved with free doxorubicin.

Differential biodistribution of nanoparticle-encapsulated drug in MPNST and UPS models

The differential benefit of CP-Dox observed between MPNST and UPS mice suggests a fundamental difference in the biology of these tumors, even with identical initiating mutations in the same genetic background. To determine whether the improved CP-Dox response represents an intrinsic property of the cancer cells or is the result of different tumor-extrinsic factors between tumors located in the muscle and nerve, we defined the concentration of the drugs needed to inhibit 50% of cell proliferation (IC_{50}) for tumor-derived cell lines. Similar to previous reports, both MPNST and UPS cells are more sensitive to free doxorubicin than CP-Dox (Supplementary Table S1). In addition, MPNST cells are more sensitive to both free doxorubicin and CP-Dox than UPS cells, and the IC_{50} for CP-Dox is approximately 5-fold lower for MPNST cells than UPS cells, which could partially contribute to the improved responses observed *in vivo*. To examine additional factors that play a role in the efficacy of CP-Dox treatment, we examined several tumor-

Published OnlineFirst July 27, 2020; DOI: 10.1158/1078-0432.CCR-19-2597

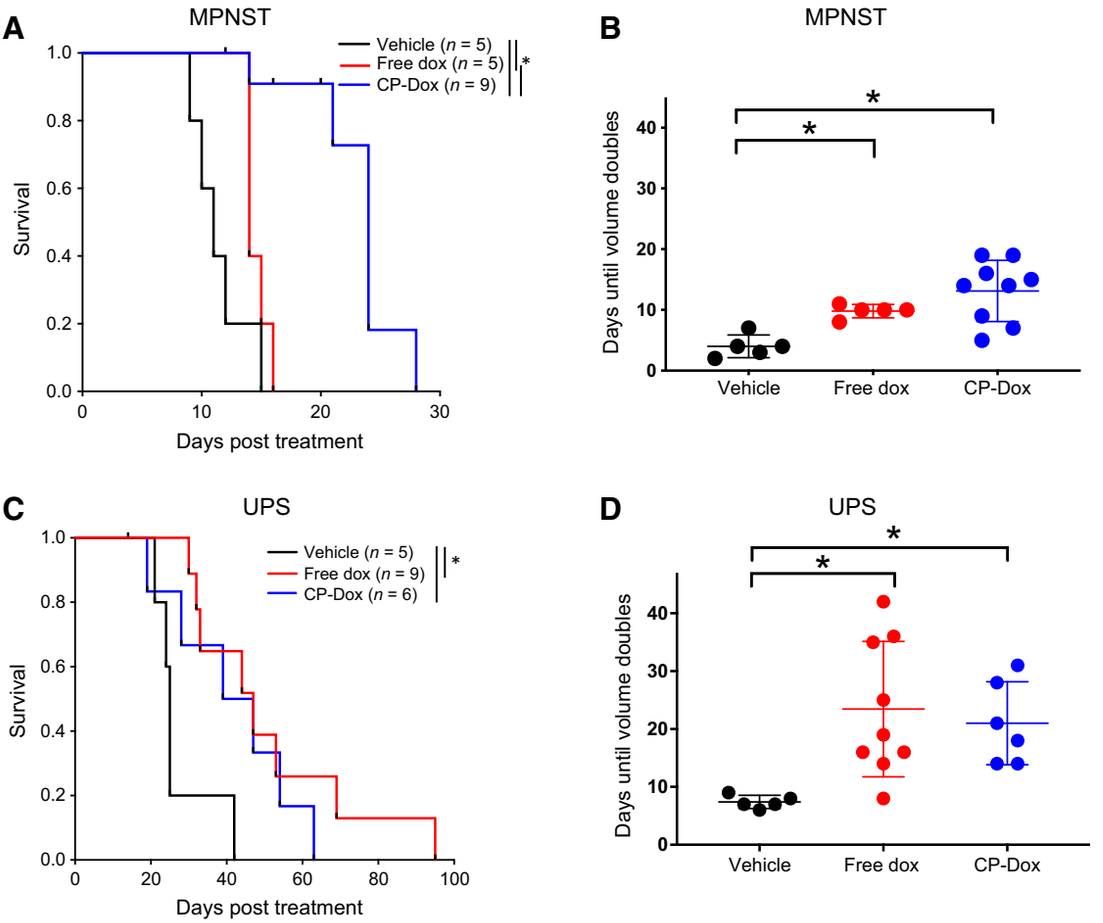

Figure 4.

CP-Dox treatment is superior to free doxorubicin in MPNSTs, but not in UPS tumors. When tumors reach 150–300 mm^3, mice receive a single bolus of vehicle, free doxorubicin, or CP-Dox, followed by caliper measurements three times per week. **A** and **B,** In MPNST-bearing mice, treatment with CP-Dox extends survival (**A**) and slows tumor growth (**B**) significantly more than vehicle or free doxorubicin. Tumor growth kinetics are reported as the number of days required for tumors to double in volume. In contrast, in UPS-bearing mice, treatment with either free doxorubicin or CP-Dox extends survival (**C**) and slows tumor growth (**D**) significantly more than vehicle alone. Tumor growth kinetics are reported as the number of days required for tumors to double in volume. A "*" denotes $P < 0.05$ from one-way ANOVA with Tukey multiple comparison test.

extrinsic factors, including improved tumor retention and immune modulation.

To examine tumor retention of the drugs, we obtained tumor, kidney, and muscle tissue from mice recently injected with 5 mg/kg of free doxorubicin or CP-Dox. Because of the native red fluorescence of doxorubicin, pharmacokinetic measurements can easily be performed on processed samples to determine the amount of drug delivered into the tumor when normalized to control tissue. At 2 hours postinjection, both CP-Dox and free doxorubicin are present at similar levels in MPNSTs relative to normal kidney (**Fig. 5A**). However, at 24 hours postinjection, the CP-Dox formulation results in significantly higher intratumoral concentrations of doxorubicin, showing the improved accumulation and retention of the nanoparticle formulation in the MPNSTs. In contrast, analysis of UPS tumors shows that similar amounts of both CP-Dox and free doxorubicin remain in the tumor for 2 hours and 24 hours postinjection (**Fig. 5C**). Similar results are seen when biodistribution data are normalized to muscle (Supplementary Fig. S3). This drug accumulation study supports the notion that CP-Dox improves survival in MPNSTs partially due to increased tumor bioavailability. Therefore, the absence of survival benefit observed with CP-Dox treatment of UPS tumors can be partially explained by the inability to improve tumor accumulation with the nanoparticle formulation in these tumors. Taken together, these data suggest that novel CP nanoparticle–based formulations of doxorubicin may be beneficial for patients with MPNST, but may not be beneficial for patients with myogenic tumors. Although these findings may in part depend on the increased growth rates of our murine sarcomas compared with the clinical disease, these results highlight the importance of examining therapeutic outcome in preclinical studies of different sarcoma subtypes and anatomic locations.

T-cell infiltration correlates with response in CP-Dox–treated tumors but is not required for full efficacy

Recent studies have implicated elevated lymphocyte activity in CP-Dox efficacy. In a transplant model of mouse 4T1 cells, antibody blocking studies demonstrated that CP-Dox–associated survival and prevention of metastasis were dependent on $CD8^+$ T cells (15). On the basis of these findings, we hypothesized that $CD8^+$ T-cell

Published OnlineFirst July 27, 2020; DOI: 10.1158/1078-0432.CCR-19-2597

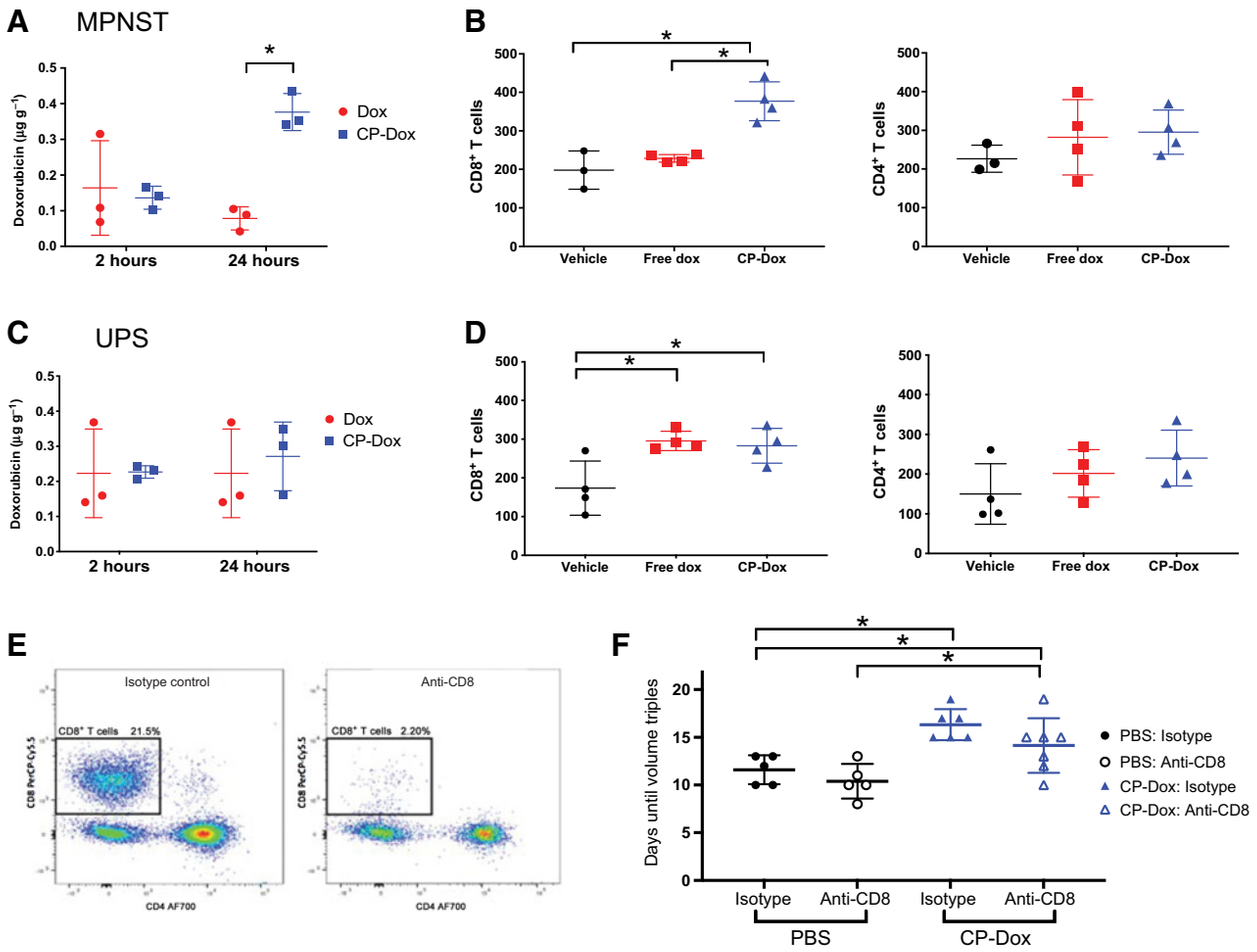

Figure 5.

CP-Dox affects biodisribution and immune infiltration in MPNSTs, but not in UPS tumors. **A,** In MPNSTs, CP-Dox levels remain elevated 24 hours after intravenous injection, whereas free doxorubicin levels remain at baseline levels. Values are normalized to kidney. **B,** Levels of $CD8^+$ T cells are elevated in terminally harvested MPNSTs treated with CP-Dox, but there is no increase of $CD8^+$ T cells in MPNSTs treated with free doxorubicin. $CD4^+$ T-cell levels are unaffected by doxorubicin treatment. **C,** In UPS tumors, CP-Dox levels remain close to baseline levels 24 hours after intravenous injection. Values are normalized to kidney. **D,** Levels of $CD8^+$ T cells are elevated in terminally harvested UPS tumors treated with either CP-Dox or free doxorubicin in comparison with vehicle alone. $CD4^+$ T-cell levels are unaffected by doxorubicin treatment. **E** and **F,** Depletion of $CD8^+$ T cells in MPNSTs does not affect the efficacy of CP-Dox. Upon tumor detection, NC mice were injected with anti-CD8 or isotype control antibody, followed by CP-Dox 24 hours later. $CD8^+$ T-cell depletion was confirmed by flow cytometry. Tumor growth kinetics are reported as the number of days required for tumors to triple in volume. A "*" denotes $P < 0.05$ from one-way ANOVA with Tukey multiple comparison test.

infiltration would correlate with improved response to doxorubicin-containing therapy. We performed IHC for $CD4^+$ and $CD8^+$ T cells on terminally harvested MPNST and UPS tumor tissue treated with either CP-Dox or free doxorubicin. In MPNSTs, $CD8^+$ T-cell infiltration increases in tumors treated with CP-Dox compared with vehicle (**Fig. 5B**). In contrast, there is no increase of $CD8^+$ T cells in MPNSTs treated with free doxorubicin. In UPS tumors, $CD8^+$ T cells are elevated in both CP-Dox and free doxorubicin-treated tumors, compared with vehicle alone (**Fig. 5D**). IHC analysis of $CD4^+$ T cells shows no statistical change in MPNSTs or UPS tumors treated with either doxorubicin formulation (**Fig. 5B** and **D**). These data raise the possibility that improved responses to doxorubicin-containing therapy are partially due to $CD8^+$ T-cell recruitment. While UPS-bearing mice have extended survival and increased $CD8^+$ T-cell infiltration in response to either drug formulation, MPNSTs show a survival benefit and elevated $CD8^+$ T-cell levels only when treated with CP-Dox. To determine whether $CD8^+$ T cells were necessary for CP-Dox efficacy in MPNSTs, we injected tumor-bearing mice with a CD8-depleting antibody prior to CP-Dox injection (**Fig. 5E** and **F**). Mice continued to receive isotype control or anti-CD8 antibody every 3–4 days until tumor harvest. CP-Dox was able to slow MPNST growth to a similar extent in both CD8-depleted and isotype control mice. These data suggest that $CD8^+$ T cells are not required for full efficacy of CP-Dox in MPNST models. Taken together, the improved response to CP-Dox in MPNSTs can be at least partially explained by higher doxorubicin delivery to the tumor, but increased immune cell recruitment is not required for full efficacy.

Published OnlineFirst July 27, 2020; DOI: 10.1158/1078-0432.CCR-19-2597

Discussion

To directly compare the preclinical efficacy of CP nanoparticle–based chemotherapeutic formulations in genetically identical tumors of different sarcoma subtypes, we generated MPNST and UPS models with deletions in *Pten, Nf1*, and *Cdkn2a* using both Cre/loxP and CRISPR/Cas9 approaches. In the MPNST model, we observed that CP-Dox significantly extends animal survival and slows tumor growth (**Fig. 4A** and **B**). To our knowledge, this is the first demonstration in a primary tumor model that CP-Dox improves response in comparison with free doxorubicin. In contrast to our observations in MPNSTs, we found that CP-Dox has no survival advantage over conventional doxorubicin in the UPS tumors (**Fig. 4C** and **D**). By developing two mouse models of sarcoma with different responses to CP-Dox, we can explore possible mechanisms contributing to drug efficacy. Our data show that improved response to CP-Dox correlates with (i) increased tumor uptake of CP-Dox versus free doxorubicin and (ii) increased $CD8^+$ T-cell infiltration into treated tumors (**Fig. 5**). However, pretreatment with an anti-CD8 antibody does not decrease the efficacy of CP-Dox in MPNSTs, suggesting $CD8^+$ T cells are not required for full efficacy of the drug in this model. Taken together, our *in vivo* studies point to an important role for enhanced biodistribution in efficacy of nanoparticle formulations and have important implications for clinical approaches in sarcoma by highlighting the context-dependent nature of therapeutic response in different sarcoma subtypes.

The hypothesis that CP-Dox is superior to free doxorubicin across many solid tumor types because the nanoparticle formulation can deliver a higher concentration of drug to the tumor (8–10) is supported by our observations in the MPNST sarcoma model. Our work raises the possibility that the EPR model of nanoparticle retention may be different in MPNSTs versus UPS tumors. In MPNSTs, CP-Dox is retained at higher levels than free doxorubicin, as predicted by the EPR theory. In contrast, both CP-Dox and free doxorubicin are retained at similar levels in UPS tumors (**Fig. 5**). This implies that while MPNSTs display the increased permeability expected for cancer-associated vasculature, UPS tumors may have vasculature that is not hyperpermable to CP-Dox to the same extent, which may explain the lack of elevated CP-Dox accumulation in these tumors. This comparison further illustrates the importance of evaluating therapies across multiple subtypes of genomically matched sarcomas.

These studies suggest the role of T cells in CP-Dox activity is context dependent. While the effect of CP-Dox in our primary model of MPNST is CD8 independent, previous studies have demonstrated that $CD8^+$ T cells are required for full efficacy of CP-Dox in a cell transplant model of breast cancer (15). Several factors could contribute to these differences including differences in immune cell function between breast cancer and sarcoma models. However, we speculate that this finding may simply reflect differences between cell transplant and primary mouse models, as studies have shown that transplant models, but not autocthonous models, demonstrate a requirement for adaptive immunity in chemotherapy responses (38–41).

We also performed a side-by-side comparison of *in vivo* models of *Pten* deletion using Cre/loxP and CRISPR/Cas9 methods. With the advent of CRISPR/Cas9 tools in cancer modeling, a direct comparison of conventional genetically engineered mice and new CRISPR/Cas9 approaches is instructive. A major advantage of classical Cre/loxP models is the ability to compare between gene dosage (loss of one copy vs. two copies). These data demonstrate that homozygous loss of *Pten* is required to accelerate MPNST or UPS tumor formation, as heterozygous *Pten* loss was not sufficient to accelerate tumor onset. Advantages of CRISPR/Cas9 somatic tumorigenesis methods include comparing distinct genetic mutations with a rapidly adaptable approach without the need for generating additional genetically engineered conditional mice and the time required for breeding schemes. For example, while the role of *Pten* loss in MPNST biology has been well established, CRISPR/Cas9 tools allow for rapid screening of other mutations in the future without the need for multiple genetic crosses. In comparing our Cre/loxP and CRISPR/Cas9 models, we determined that *Pten* deletion can accelerate sarcoma initiation in both MPNST and UPS models. As expected for *Pten* deletion and PI3K pathway activation, levels of phosphorylated AKT are observed with *Pten* deletion in cell lines derived from all tumors. However, there are several differences in activation of cellular signaling pathways downstream of PI3K between the different models. For example, PI3K-mediated phospho-S6 induction is observed only in tumor-derived cell lines where *Pten* is mutated by CRISPR/Cas9 technology, not with Cre/loxP technology, and the upregulation of phospho-ERK is detected only in some cell lines derived from UPS tumors, but not MPNSTs.

There are several hypotheses that could explain the differences in *Pten* deletion–driven phenotypes across the multiple models. First, the *Rosa26-LSL-Cas9*–containing mice are on a different genetic background that could be more sensitive to *Pten* deletion, resulting in altered cellular signaling. Second, constitutive activation of the Cas9 enzyme could increase phospho-S6 levels in tumors from LSL-Cas9; NC mice, potentially influencing signaling cascades. Third, *Pten* deletion may increase phospho-ERK levels in UPS tumors due to relatively low levels in *Pten* wild-type tumors, whereas phospho-ERK levels are already elevated in *Pten* wild-type MPNSTs, and therefore *Pten* loss may be unable to activate the MAPK/ERK pathway beyond baseline levels.

Efforts are underway to test CP-based formuations in other animal models. A recent study of the pharmacokinetics of CP-Dox in dogs showed that CP-Dox nanoparticles circulate far longer in systemic circulation than free drugs, similar to the data obtained in mice (33). These results are encouraging, given the recent interest in canine models for preclinical studies (42–44), and suggest that the better efficacy of CP-Dox nanoparticle compared with free drug seen in mouse models may translate to humans. Current studies are focused on further improving the bioavailability of drugs by designing newer CP nanoparticles that present multiple copies of an albumin-binding protein domain on their exterior, facilitating binding of endogenous albumin to sheath the nanoparticle with an albumin corona (33). Encouraging results in a mouse transplanted colon cancer model suggest that these albumin-coated nanoparticles represent the "next-generation" of CP-Dox formulations. Our study in primary mouse models of MPNST and UPS suggests that CP-Dox and nanopariticle formulations in general may be a promising treatment approach for patients with MPNSTs. Given the diversity of biology across STS subtypes, there is increasing appreciation that systemic sarcoma therapies need to be tailored to each subtype. The development of new approaches to model patient-relevant mutations in preclinical models of different sarcoma subtypes will accelerate bench-to-bedside studies of new treatment paradigms.

Disclosure of Potential Conflicts of Interest

R.D. Dodd reports grants and nonfinancial support from University of Iowa during the conduct of the study. A. Scherer reports grants from University of Iowa during the conduct of the study. W.R. Gutierrez reports grants from University of Iowa during the conduct of the study. V.R. Stephens reports grants from University of Iowa (salary support) during the conduct of the study. M. Chen

Published OnlineFirst July 27, 2020; DOI: 10.1158/1078-0432.CCR-19-2597

reports grants from NIH/NCI (F30CA206424, T32GM007171) during the conduct of the study. E.M. Mastria reports grants from NIH during the conduct of the study. D.G. Kirsch reports grants from NCI (R35CA197616) during the conduct of the study; other from Lumicell (member of scientific advisory board), Lumicell (stock, stock options), Lumicell (consultant), Lumicell (patents), Lumicell (royalties), Xrad Therapeutics (cofounder), Xrad Therapeutics (own Stock), Xrad Therapeutics (research support); grants from Lumicell (research support), Merck (support for clinical trial), Eli Lilly (research support), Bristol-Myers Squibb (research support), and Varian Medical Systems (research support) outside the submitted work. No potential conflicts of interest were disclosed by the other authors.

Authors' Contributions

R.D. Dodd: Conceptualization, data curation, formal analysis, supervision, funding acquisition, investigation, visualization, methodology, writing–original draft, project administration, writing–review and editing. **A. Scherer:** Data curation, formal analysis, investigation, methodology, writing–review and editing. **W. Huang:** Data curation, formal analysis, investigation, writing–review and editing. **G.R. McGivney:** Data curation, formal analysis, investigation, writing–review and editing. **W.R. Gutierrez:** Investigation, writing–review and editing. **E.A. Laverty:** Data curation, investigation, writing–review and editing. **K.A. Ashcraft:** Formal analysis, investigation, writing–review and editing. **V.R. Stephens:** Data curation, formal analysis, investigation, writing–review and editing. **P. Yousefpour:** Resources, validation, investigation, methodology, writing–review and editing. **S. Saha:** Resources, validation, methodology, writing–review and editing. **V. Knepper-Adrian:** Investigation, methodology, writing–review and editing. **W. Floyd:** Formal analysis, investigation, writing–review and editing. **M. Chen:** Formal analysis, investigation, writing–review and editing. **Y. Ma:** Investigation, writing–review and editing. **E.M. Mastria:** Resources, validation, methodology, writing–review and editing. **D.M. Cardona:** Formal analysis, investigation, writing–review and editing. **W.C. Eward:** Investigation, methodology, writing–review and editing. **A. Chilkoti:** Conceptualization, resources, supervision, writing–original draft, writing–review and editing. **D.G. Kirsch:** Conceptualization, supervision, funding acquisition, writing–original draft, writing–review and editing.

Acknowledgments

The authors would like to acknowledge personnel in the core facilities (Flow Cytometry, Central Microscopy, Genomics and Biostatistics) at the University of Iowa Carver College of Medicine and Holden Comprehensive Cancer Center for their assistance. We would like to thank the labs of Drs. Michael Henry, Christopher Stipp and David Gordon for their sharing of reagents and critical feedback. This work is supported by a Department of Defense CDMRP NF1 New Investigator Award (to D.G. Kirsch), R35CA197616 (to D.G. Kirsch), F30CA206424 (to M. Chen), T32GM007171 (to M. Chen) T32GM0677954 (to W. R. Gutierrez), T32GM007337 (to W.R. Gutierrez), and an NCI Core Grant P30 CA086862 (University of Iowa Holden Comprehensive Cancer Center).

The costs of publication of this article were defrayed in part by the payment of page charges. This article must therefore be hereby marked *advertisement* in accordance with 18 U.S.C. Section 1734 solely to indicate this fact.

Received August 7, 2019; revised April 7, 2020; accepted July 20, 2020; published first July 27, 2020.

References

1. Judson I, Verweij J, Gelderblom H, Hartmann JT, Schöffski P, Blay JY, et al. Doxorubicin alone versus intensified doxorubicin plus ifosfamide for first-line treatment of advanced or metastatic soft-tissue sarcoma: a randomised controlled phase 3 trial. Lancet Oncol 2014;15:415–23.
2. Tap WD, Jones RL, Van Tine BA, Chmielowski B, Elias AD, Adkins D, et al. Olaratumab and doxorubicin versus doxorubicin alone for treatment of soft-tissue sarcoma: an open-label phase 1b and randomised phase 2 trial. Lancet 2016;388:488–97.
3. Seddon B, Strauss SJ, Whelan J, Leahy M, Woll PJ, Cowie F, et al. Gemcitabine and docetaxel versus doxorubicin as first-line treatment in previously untreated advanced unresectable or metastatic soft-tissue sarcomas (GeDDiS): a randomised controlled phase 3 trial. Lancet Oncol 2017;18:1397–410.
4. Lorigan P, Verweij J, Papai Z, Rodenhuis S, Le Cesne A, Leahy MG, et al. Phase III trial of two investigational schedules of ifosfamide compared with standard-dose doxorubicin in advanced or metastatic soft tissue sarcoma: a European Organisation for Research and Treatment of Cancer Soft Tissue and Bone Sarcoma Group Study. J Clin Oncol 2007;25:3144–50.
5. Barretina J, Taylor BS, Banerji S, Ramos AH, Lagos-Quintana M, DeCarolis PL, et al. Subtype-specific genomic alterations define new targets for soft-tissue sarcoma therapy. Nat Genet 2010;42:715–21.
6. Lee W, Teckie S, Wiesner T, Ran L, Granada CN, Lin M, et al. PRC2 is recurrently inactivated through EED or SUZ12 loss in malignant peripheral nerve sheath tumors. Nat Genet 2014;46:1227–32.
7. Maki RG, D'Adamo DR, Keohan ML, Saulle M, Schuetze SM, Undevia SD, et al. Phase II study of sorafenib in patients with metastatic or recurrent sarcomas. J Clin Oncol 2009;27:3133–40.
8. MacKay JA, Chen M, McDaniel JR, Liu W, Simnick AJ, Chilkoti A. Self-assembling chimeric polypeptide–doxorubicin conjugate nanoparticles that abolish tumours after a single injection. Nat Mater 2009;8:993–9.
9. McDaniel JR, MacEwan SR, Dewhirst M, Chilkoti A. Doxorubicin-conjugated chimeric polypeptide nanoparticles that respond to mild hyperthermia. J Control Release 2012;159:362–7.
10. Betre H, Liu W, Zalutsky MR, Chilkoti A, Kraus VB, Setton LA. A thermally responsive biopolymer for intra-articular drug delivery. J Control Release 2006; 115:175–82.
11. Maeda H. The enhanced permeability and retention (EPR) effect in tumor vasculature: the key role of tumor-selective macromolecular drug targeting. Adv Enzyme Regul 2001;41:189–207.
12. Mastria EM, Chen M, McDaniel JR, Li X, Hyun J, Dewhirst MW, et al. Doxorubicin-conjugated polypeptide nanoparticles inhibit metastasis in two murine models of carcinoma. J Control Release 2015;208:52–8.
13. Bhattacharyya J, Bellucci JJ, Weitzhandler I, McDaniel JR, Spasojevic I, Li X, et al. A paclitaxel-loaded recombinant polypeptide nanoparticle outperforms Abraxane in multiple murine cancer models. Nat Commun 2015;6:7939.
14. Bhattacharyya J, Ren XR, Mook RA, Wang J, Spasojevic I, Premont RT, et al. Niclosamide-conjugated polypeptide nanoparticles inhibit Wnt signaling and colon cancer growth. Nanoscale 2017;9:12709–17.
15. Mastria EM, Cai LY, Kan MJ, Li X, Schaal JL, Fiering S, et al. Nanoparticle formulation improves doxorubicin efficacy by enhancing host antitumor immunity. J Control Release 2018;269:364–73.
16. Kim S, Dodd RD, Mito JK, Ma Y, Kim Y, Riedel RF, et al. Efficacy of phosphatidylinositol-3 kinase inhibitors in a primary mouse model of undifferentiated pleomorphic sarcoma. Sarcoma 2012;2012:680708.
17. Dodd RD, Mito JK, Eward WC, Chitalia R, Sachdeva M, Ma Y, et al. NF1 deletion generates multiple subtypes of soft-tissue sarcoma that respond to MEK inhibition. Mol Cancer Ther 2013;12:1906–17.
18. Dodd RD, Lee CL, Overton T, Huang W, Eward WC, Luo L, et al. NF1+/− Hematopoietic cells accelerate malignant peripheral nerve sheath tumor development without altering chemotherapy response. Cancer Res 2017;77:4486–97.
19. Kirsch DG, Dinulescu DM, Miller JB, Grimm J, Santiago PM, Young NP, et al. A spatially and temporally restricted mouse model of soft tissue sarcoma. Nat Med 2007;13:992–7.
20. Mito JK, Riedel RF, Dodd L, Lahat G, Lazar AJ, Dodd RD, et al. Cross species genomic analysis identifies a mouse model as undifferentiated pleomorphic sarcoma/malignant fibrous histiocytoma. PLoS One 2009;4:e8075.
21. Cancer Genome Atlas Research Network. Comprehensive and integrated genomic characterization of adult soft tissue sarcomas. Cell 2017;171:950–65.e28.
22. George S, Miao D, Demetri GD, Adeegbe D, Rodig SJ, Shukla S, et al. Loss of PTEN is associated with resistance to anti-PD-1 checkpoint blockade therapy in metastatic uterine leiomyosarcoma. Immunity 2017;46:197–204.
23. Bradtmöller M, Hartmann C, Zietsch J, Jäschke S, Mautner VF, Kurtz A, et al. Impaired Pten expression in human malignant peripheral nerve sheath tumours. PLoS One 2012;7:e47595.
24. Gregorian C, Nakashima J, Dry SM, Nghiemphu PL, Smith KB, Ao Y, et al. PTEN dosage is essential for neurofibroma development and malignant transformation. Proc Natl Acad Sci U S A 2009;106:19479–84.

25. Guijarro MV, Dahiya S, Danielson LS, Segura MF, Vales-Lara FM, Menendez S, et al. Dual Pten/Tp53 suppression promotes sarcoma progression by activating Notch signaling. Am J Pathol 2013;182:2015–27.
26. Buchakjian MR, Merritt NM, Moose DL, Dupuy AJ, Tanas MR, Henry MD. A Trp53fl/flPtenfl/fl mouse model of undifferentiated pleomorphic sarcoma mediated by adeno-Cre injection and *in vivo* bioluminescence imaging. PLoS One 2017;12:e0183469.
27. Keng VW, Rahrmann EP, Watson AL, Tschida BR, Moertel CL, Jessen WJ, et al. PTEN and NF1 inactivation in Schwann cells produces a severe phenotype in the peripheral nervous system that promotes the development and malignant progression of peripheral nerve sheath tumors. Cancer Res 2012;72:3405–13.
28. Lesche R, Groszer M, Gao J, Wang Y, Messing A, Sun H, et al. Cre/loxP-mediated inactivation of the murine Pten tumor suppressor gene. Genesis 2002;32:148–9.
29. Platt RJ, Chen S, Zhou Y, Yim MJ, Swiech L, Kempton HR, et al. CRISPR-Cas9 knockin mice for genome editing and cancer modeling. Cell 2014;159:440–55.
30. Dodd RD, Añó L, Blum JM, Li Z, Van Mater D, Kirsch DG. Methods to generate genetically engineered mouse models of soft tissue sarcoma. Methods Mol Biol 2015;1267:283–295.
31. Huang J, Chen M, Whitley MJ, Kuo HC, Xu ES, Walens A, et al. Generation and comparison of CRISPR-Cas9 and Cre-mediated genetically engineered mouse models of sarcoma. Nat Commun 2017;8:15999.
32. Sánchez-Rivera FJ, Papagiannakopoulos T, Romero R, Tammela T, Bauer MR, Bhutkar A, et al. Rapid modelling of cooperating genetic events in cancer through somatic genome editing. Nature 2014;516:428–31.
33. Yousefpour P, McDaniel JR, Prasad V, Ahn L, Li X, Subrahmanyan R, et al. Genetically encoding albumin binding into chemotherapeutic-loaded polypeptide nanoparticles enhances their antitumor efficacy. Nano Lett 2018;18:7784–93.
34. Maresch R, Mueller S, Veltkamp C, Öllinger R, Friedrich M, Heid I, et al., Multiplexed pancreatic genome engineering and cancer induction by transfection-based CRISPR/Cas9 delivery in mice. Nat Commun 2016;7:10770.
35. Lee YR, Chen M, Pandolfi PP. The functions and regulation of the PTEN tumour suppressor: new modes and prospects. Nat Rev Mol Cell Biol 2018;19:547–62.
36. Caunt CJ, Sale MJ, Smith PD, Cook SJ. MEK1 and MEK2 inhibitors and cancer therapy: the long and winding road. Nat Rev Cancer 2015;15:577–92.
37. Bhattacharyya J, Weitzhandler I, Ho SB, McDaniel JR, Li X, Tang L, et al. Encapsulating a hydrophilic chemotherapeutic into rod-like nanoparticles of a genetically encoded asymmetric triblock polypeptide improves its efficacy. Adv Funct Mater 2017;27:1605421.
38. Ciampricotti M, Hau C, Doornebal C, Jonkers J, de Visser K. Chemotherapy response of spontaneous mammary tumors is independent of the adaptive immune system. Nat Med 2012;18:344–6.
39. Apetoh L, Ghiringhelli F, Tesniere A, Obeid M, Ortiz C, Criollo A, et al. Toll-like receptor 4–dependent contribution of the immune system to anticancer chemotherapy and radiotherapy. Nat Med 2007;13:1050–9.
40. Obeid M, Tesniere A, Ghiringhelli F, Fimia GM, Apetoh L, Perfettini JL, et al. Calreticulin exposure dictates the immunogenicity of cancer cell death. Nat Med 2007;13:54–61.
41. Ghiringhelli F, Apetoh L, Tesniere A, Aymeric L, Ma Y, Ortiz C, et al. Activation of the NLRP3 inflammasome in dendritic cells induces IL-1β–dependent adaptive immunity against tumors. Nat Med 2009;15:1170–8.
42. Thamm DH. Canine cancer: strategies in experimental therapeutics. Front Oncol 2019;9:1257.
43. Thamm DH, Kurzman ID, King I, Li Z, Sznol M, Dubielzig RR, et al. Systemic administration of an attenuated, tumor-targeting salmonella typhimurium to dogs with spontaneous neoplasia: phase i evaluation. Clin Cancer Res 2005;11:4827–34.
44. Toso JF, Gill VJ, Hwu P, Marincola FM, Restifo NP, Schwartzentruber DJ, et al. Phase I study of the intravenous administration of attenuated salmonella typhimurium to patients with metastatic melanoma. J Clin Oncol 2002;20:142–52.

Published OnlineFirst July 27, 2020; DOI: 10.1158/1078-0432.CCR-19-2597

Clinical Cancer Research

Tumor Subtype Determines Therapeutic Response to Chimeric Polypeptide Nanoparticle–based Chemotherapy in *Pten*-deleted Mouse Models of Sarcoma

Rebecca D. Dodd, Amanda Scherer, Wesley Huang, et al.

Clin Cancer Res 2020;26:5036-5047. Published OnlineFirst July 27, 2020.